Original Article

MOLECULAR METABOLISM

Dynamic changes in β-cell [Ca^{2+}] regulate NFAT activation, gene transcription, and islet gap junction communication

Jose G. Miranda [1], Wolfgang E. Schleicher [1], Kristen L. Wells [3], David G. Ramirez [1], Samantha P. Landgrave [2], Richard K.P. Benninger [1,2,3,*]

ABSTRACT

Objective: Diabetes occurs because of insufficient insulin secretion due to β-cell dysfunction within the islet of Langerhans. Elevated glucose levels trigger β-cell membrane depolarization, action potential generation, and slow sustained free-Ca^{2+} ([Ca^{2+}]) oscillations, which trigger insulin release. Nuclear factor of activated T-cell (NFAT) is a transcription factor, which is regulated by the increases in [Ca^{2+}] and calceineurin (CaN) activation. NFAT regulation links cell activity with gene transcription in many systems and regulates proliferation and insulin granule biogenesis within the β-cell. However, the link between the regulation of β-cell electrical activity and oscillatory [Ca^{2+}] dynamics with NFAT activation and downstream transcription is poorly understood. Here, we tested whether dynamic changes to β-cell electrical activity and [Ca^{2+}] regulate NFAT activation and downstream transcription.

Methods: In cell lines, mouse islets, and human islets, including those from donors with type 2 diabetes, we applied both agonists/antagonists of ion channels together with optogenetics to modulate β-cell electrical activity. We measured the dynamics of [Ca^{2+}] and NFAT activation as well as performed whole transcriptome and functional analyses.

Results: Both glucose-induced membrane depolarization and optogenetic stimulation triggered NFAT activation as well as increased the transcription of NFAT targets and intermediate early genes (IEGs). Importantly, slow, sustained [Ca^{2+}] oscillation conditions led to NFAT activation and downstream transcription. In contrast, in human islets from donors with type2 diabetes, NFAT activation by glucose was diminished, but rescued upon pharmacological stimulation of electrical activity. NFAT activation regulated *GJD2* expression and increased Cx36 gap junction permeability upon elevated oscillatory [Ca^{2+}] dynamics. However, it is unclear if NFAT directly binds the *GJD2* gene to regulate expression.

Conclusions: This study provides an insight into the specific patterns of electrical activity that regulate NFAT activation, gene transcription, and islet function. In addition, it provides information on how these factors are disrupted in diabetes.

Keywords NFAT; Ca^{2+}; Optogenetics; Transcription

1. INTRODUCTION

β-cells play a crucial role in maintaining glucose homeostasis by secreting insulin that promotes glucose uptake and maintains glucose homeostasis. Diabetes, a disease afflicting >400M people worldwide, generally results from β-cells dysfunction/death and insufficient release of insulin. Following the elevations in blood glucose levels, β-cells undergo a series of steps such as metabolism of glucose to elevate ATP, closure of ATP-sensitive K^+ (K_{ATP}) channels, depolarization of the membrane, which activates voltage gated calcium (Ca^{2+}) channels, and elevated cytosolic free [Ca^{2+}] activity that triggers insulin granule exocytosis and the release of insulin [1–3]. Additional pathways (termed as 'amplifying pathways') further enhance the release of insulin upon Ca^{2+} triggering. In type 2 diabetes (T2D), these pathways are disrupted in the β-cells that can explain the insufficient release of insulin and altered glucose homeostasis [4]. However, the exact mechanisms underlying β-cells dysfunction in diabetes are still unclear.

In islets, intra-cellular free Ca^{2+} activity ([Ca^{2+}]) is closely linked to electrical activity of the β-cell. Insulin is secreted in discrete pulses, which is closely tied to oscillations in [Ca^{2+}] and bursts of action potentials [5]. Pulsatile insulin release facilitates effective insulin action and glucose lowering [6–8]. Connexin-36 (Cx36) gap junctions coordinate membrane potential between β-cells within the islet. As a result, [Ca^{2+}] oscillations are synchronized across the islet, and insulin is released from the whole islet in discrete pulses [9]. Thus, the regulation of [Ca^{2+}] dynamics is a critical aspect of islet function.

While [Ca^{2+}] is important for insulin granule release, its role as a secondary messenger can also affect gene transcription [10]. Several

[1]Department of Bioengineering, University of Colorado Anschutz Medical Campus, Aurora CO, 80045, USA [2]Program in Cell Biology, Stem Cell and Development, University of Colorado Anschutz Medical Campus, Aurora, CO, 80045, USA [3]Barbara Davis Center for Childhood Diabetes, University of Colorado Anschutz Medical Campus, Aurora, CO, 80045, USA

*Corresponding author. Department of Bioengineering, University of Colorado Anschutz Medical Campus, Aurora CO, 80045, USA. E-mail: richard.benninger@cuanschutz.edu (R.K.P. Benninger).

Received February 26, 2021 • Revision received December 28, 2021 • Accepted December 29, 2021 • Available online 31 December 2021

https://doi.org/10.1016/j.molmet.2021.101430

transcription factors mediate Ca^{2+}-regulated gene transcription, such as CREB and c-Fos, among others [11—15]. The serine/threonine phosphatase calcineurin (CaN) is activated by [Ca^{2+}], which dephosphorylates its downstream target, nuclear factor of activated T-cell (NFAT). NFAT subsequently translocates to the nucleus to initiate the transcription of several genes [16—19]; thereby linking cell activity with gene transcription. This has critical importance in several systems to initiate remodeling, such as in activated T-cells or potentiating neuronal synapses [20]. Within the islet, NFAT regulates the genes involved in β-cell function, including glucose sensing and granule formation [16,18,21,22]. NFAT also regulates the genes involved in proliferation, with chemical activators of NFAT stimulating β-cell proliferation. Although there is significant information regarding β-cell pathways activated by NFAT, it is unclear what physiological conditions within the β-cell lead to NFAT activation, particularly the link with stimulus-secretion coupling.

Here, we examine the link between the regulation of β-cell electrical activity and oscillatory [Ca^{2+}], with NFAT activation and downstream transcription. We controlled the dynamics of islet electrical activity using either specific agonists/antagonists of ion channels together with optogenetics via light activation of the cation channel ChR2. Using cell lines, mouse primary islets, and human primary islets, we determined the levels and dynamics of [Ca^{2+}] under which NFAT could be activated and downstream gene transcription modified. We further tested whether altered Ca^{2+} regulation in models of T2D and human T2D impacted NFAT activation, and whether this can be normalized through exogenous control of [Ca^{2+}]. Thus, overall, this article provides an insight into the specific activity patterns that regulate NFAT activation and gene transcription within both the healthy and diabetic islets.

2. MATERIALS AND METHODS

2.1. Animals

All mouse experiments were performed in compliance with the University of Colorado Anschutz Medical Campus International Animal Care and Use Committee (IACUC). Mice were provided with water and food *ad libitum* and were housed in an environment with adequate temperature control with a 12-h light/dark cycle. C57BL/6NHsd (C57BL/6) mice were obtained from Envigio. Rosa26-ChR2(H134R)-YFP; Pdx-Cre mice [23] were bred in house.

2.2. Chemicals and reagents

Diazoxide, glibenclamide, quercetin, bovine serum albumen (BSA), β-mercaptoethanol, tetraethylammonium (TEA), D-(+)-glucose, and thapsigargin were purchased from Sigma—Aldrich (St. Louis, MO). FK506 was purchased from Enzo Life Sciences (Farmingdale, NY). SYBR Green qPCR Master Mix was purchased from Thermo Fisher Scientific. Calcium indicator Rhod2-AM was purchased from AAT-Bioquest (Sunnyvale, CA). mCherry-NFATc3, GFP-NFATc1, GFP-NFATc2, GFP-NFATc3, and GFP-NFATc4 constructs were gifted by Dr. Mark Dell'Aqua (University of Colorado Anschutz Medical Campus). ChR2(H134R)-YFP plasmid was obtained from Addgene. Adenovirus particles containing mCherry-NFATc3 were prepared by the Diabetes, Obesity and Metabolism Institute, Icahn School of medicine at Mount Sinai. Cytosolic D3cpV FRET probe was gifted by Dr. Amy E. Palmer (University of Colorado Boulder).

2.3. Cell culture

Mouse insulinoma cells (MIN6) were grown in Dulbecco's modified eagle's medium (DMEM, Corning) supplemented with 10% (v/v) fetal bovine serum (FVS) (Gibco), 100 U/mL penicillin, 100 μg/mL streptomycin (Gibco), and 60 μM freshly added β-mercaptoethanol. Cells were incubated at 37 °C in 5% CO_2 in a humidified controlled environment, and the medium was changed in every 2—3 days. Once the cells were approximately 90—95% confluent, they were split and seeded onto 3.5 cm glass bottom imaging dishes (35 mm petri-dishes, No1.5 cover glass, Corning, Ashland, MA) until they were approximately 75% confluent. At this point, 2 μg of mCherry-NFATc3, ChR2(H134R)-YFP, and/or D3cpV plasmid DNA were transiently transfected using lipofectamine 2000 (Invitrogen) mixed with OPTI-Mem (Gibco). This included incubating lipofectamine 2000 and OPTI-Mem for 15 min followed by the addition of DNA and incubated for 45 min. The medium was changed before adding the transfection cocktail to MIN6 cells.

2.4. Islet isolation, culture, and treatments

Islets were isolated from 12- to 16-week-old mice, as previously described [24,25]. After pancreas dissection, digestion, and islet hand picking, the islets were transduced with 5 μL of adenovirus titer $1.4*10^9$ plaque forming units (pfu) containing mCherry-NFATc3 for 3.5 h at 37 °C with 5% CO_2 in a humidified environment in Roswell Park Media Institute (RPMI)-1640 media with 10% (v/v) FBS, 100 U/mL penicillin, and 100 μg/mL streptomycin. After adenoviral incubation, the islets were transferred to fresh RPMI-1640 media and incubated at 37 °C overnight before starting the experiments.

Islets from healthy and type 2 diabetic (T2D) human donors were obtained from the Integrated Islet Distribution Program (IIDP). IDs for human islets obtained from donors without diabetes: AEFB055, AEGR353, AEHW247, AEHI491, AEIM290, AEJT193B, AEI1395, AEJQ100, and AEFO120; IDs for islets from donors with T2D: AEHL151, AEKH055, AELK219, AFBP453, AFBE414, and AFBK273. The average viability for healthy and T2D islets was 92% and 96% respectively. One set of islets from a donor with T2D was obtained from The University of Alberta Edmonton, Alberta, Canada (ID: R259). Upon arrival islets were incubated in CMRL 1066 medium (Corning) at 37 °C, for 1h prior to mCherry-NFATc3 transduction. Transduction of mCherry-NFATc3 into healthy and T2D patient islets was done as stated above using mouse islets.

For pro-inflammatory cytokine treatment, mouse and healthy human islets were treated for 2 h before the experiment using vehicle control or a cytokine cocktail mixture specific for each mouse and human, consisting of 5 ng/mL of recombinant interleukin-1β (IL-1β, R&D Systems, Minneapolis, MN), 10 ng/mL recombinant tumor necrosis factor-α (TNF-α, R&D Systems), and 100 ng/mL of recombinant interferon-γ (IFN-γ, R&D Systems) in RPMI-1640 media for 25 min. Islets were imaged in solution supplemented with this cocktail. Mouse cytokine cocktail was used on MIN6 cells and incubated for 2 h prior to the start of the experiment in DMEM media. MIN6, mouse and human islets were treated with 250 μM diazoxide or 1 μM FK506 in DMEM or RPMI-1640 media for 2 h prior to the start of the experiment and which was maintained constant in the imaging solution throughout the experiment. Human T2D islets were treated with 100 μM glibenclamide or 20 μM quercetin acutely post-start of experiment. MIN6 cells, healthy mouse, human islets, and islets from the donors of T2D were treated with 1 μM thapsigargin and added to cells or islets 5 min after the start of the experiment.

2.5. MIN6 and mouse islets calcium indicator staining

To measure [Ca^{2+}] changes in MIN6 cells, we used the Förster Resonance Energy Transfer (FRET) D3cpV probe. MIN6 cells were seeded onto glass bottom imaging dishes and transfected with D3cpV, as described earlier. Imaging of MIN6 with D3cpV was done 24—48 h post transfection under low and high glucose or incubated with either

250 μM diazoxide or 1 μM FK506 for 2 h prior to imaging and during imaging.

To measure [Ca^{2+}] changes in MIN6 and β-cell specific ChR2(H134R)-YFP expressing mouse islets, we used the small molecule dye Rhod2-AM. MIN6 cells were seeded onto glass bottom imaging dishes and transfected with ChR2-YFP as described earlier. Prior to imaging, cells were incubated with 4 μM Rhod2-AM in imaging solution for 1—2 h at room temperature in a dark environment. Prior to imaging, cells were briefly washed with imaging solution and imaged in imaging solution supplemented with 2 mM glucose. Mouse islets containing ChR2-YFP β-cell were imaged two days post isolation. Islets were placed in a 35 mm dish and stained with Rhod2-AM as described earlier using MIN6 cells. Islets were placed in a rotating table with slow-to-medium constant motion. After Rhod2-AM islet incubation, islets were placed in glass bottom imaging dishes.

2.6. Live-cell microscopy imaging and analysis

Post-transfection/infection, cells or islets were imaged using BMHH imaging solution (125 mM NaCl, 5.7 mM KCl, 2.5 mM $CaCl_2$, 1.2 mM $MgCl_2$, 10 mM HEPES) pH 7.4 supplemented with 0.1% BSA and 2 mM glucose, 11 mM glucose (for islets), or 20 mM glucose plus 20 mM tetraethylammonium (TEA) (for MIN6 cells, with TEA required to generate large coordinated Ca^{2+} oscillations [26—28]. An Eclipse-Ti wide field microscope (Nikon) with a Nikon Plan Apo 20×/0.75 NA air objective or Nikon Apo LWD 40×/1.15 NA water immersion objective was used for islets and MIN6 cells, respectively. A Lambda 10^{-3} filter switcher and shutter controller were used with a Lambda LB-LS/30 Xenon arc lamp (Sutter Instruments). Images were acquired at 1 frame/15 s for 5 m at low glucose and 1 frame/15 s for 25 m after high-glucose stimulation using an Andor CCD camera, with Nikon Elements software to operate the system. For optogenetic stimulation, two pulse protocols were designed and imaging experiments were performed at low (2 mM) glucose. For the first protocol, termed 'slow pulse' protocol, ChR2(H134R)-YFP was activated at 1 frame/sec for 1 min followed 5 min of non-ChR2-YFP activation. This was repeated 5 times for the total duration of 30 min. For the second protocol, termed fast pulse protocol, ChR2-YFP was activated at 1 frame/sec for 30s followed 3 min of non-ChR2-YFP activation. This was repeated 8 times for a total duration of 30 min.

NFAT translocation in cells and islets was analyzed by drawing a region of interest in the cytosol and the nucleus of cells exhibiting fluorescence. GFP or mCherry fluorescent counts were collected frame by frame, and the nuclear fluorescent signal was divided over the cytosolic fluorescent signal $\left(\text{Nucleus fluorescence}/\text{Cytosolic fluorescence} = \text{Ratio}\right)$. Time courses were normalized to the pre-stimulation signal ratio.

For D3cpV experiments, the FRET ratio $\left(\text{FRET}/\text{CFP} = \text{FRET Ratio}\right)$ was calculated by dividing FRET signal (YFP channel signal upon CFP excitation) by CFP signal (CFP channel signal upon CFP excitation) and plotted over time. Rhod2-AM and ChR2-YFP [Ca^{2+}] experimental analysis in MIN6 cells was normalized to the pre-stimulation signal, followed by normalization to a double exponential regression curve (to account for photobleaching). Rhod2-AM and ChR2-YFP Ca^{2+} experimental analysis in mouse islets were also normalized to the pre-stimulation signal, followed by normalization to a linear regression curve.

2.7. Immunofluorescence imaging and analysis

Mouse islets were isolated and transduced with mCherry-NFATc3 adenoviral particles as described earlier. At 24 h post transduction, the islets were incubated in BMHH pH 7.4 supplemented with 2 mM or 11 mM glucose and incubated at 37 °C with 5% CO_2 in a humidified environment for 30 min. Following incubation, islets were pooled together into a 1.5 mL Eppendorf tube and incubated with 4% paraformaldehyde in ice for 15—20 min. Islets were then placed in 2% agarose until solidified. Human islets were left to recover for a minimum of 2 h upon receipt, prior to mCherry-NFATc3 transduction and low and high glucose incubation as above. Human islets were pooled and treated as with mouse islets prior to placing them into agarose. Agarose-embedded mouse or human islets were placed in O.C.T. compound and 10 μM slices were cut on a microtome and placed onto cover slides. Slides with islet sections were incubated in PBS pH 7.4 briefly followed by blocking with 5% BSA-PBS pH 7.4 for 1 h at room temperature (RT). After blocking, islet sections were incubated, with either insulin-AF 488 (1:50 dilution; Fisher Scientific) or glucagon-AF488 (1:100; R&D Systems), in 1% BSA-PBS pH 7.4 for 90 min at RT covered from ambient light. Following antibody incubation, 2 washes were performed with PBS pH 7.4 followed by mounting cover slips with DAPI-fluoromount G and storing slides at RT in a dark environment overnight. Slides were imaged on a confocal microscope (LSM800, Zeiss). Fluorescent intensity was determined in the cytosol and nucleus of mCherry-NFATc3 stained cells, as described earlier. In either Ins^{+} or Gcg^{+} immunostained cells, the ratio $\left(\text{nucleus fluorescence}/\text{cytosol fluorescence}\right)$ was then determined.

2.8. RNA extraction, qPCR, and RNAseq

Islets isolated from 10 to 12 C57BL/6NHsd (C57BL/6) mice aged 8 weeks were used for RNA extraction. Islets were collected as stated in the previous sections and given overnight recovery incubated in RPMI-1640 media. Islets were pooled together, and batches of at least 250 islets were used per treatment. Batches were then treated with one of four treatments: 2 mM glucose, 11 mM glucose, 11 mM glucose + diazoxide, or 11 mM glucose + FK506 for 4 h. Batches treated with diazoxide or FK506 were respectively incubated with either 250 μM diazoxide or 1 μM FK506 at 2 mM glucose for 1 h prior to glucose elevation. Following treatment and incubation, islets were placed in a 1.5 mL tube, briefly spun down, and supernatant removed without disturbing islets. RNA was extracted using RNeasy® Micro Kit, and cDNA was synthesized using Omniscript RT Kit according to the manufacturer's instructions. For qPCR reaction 1 μL of cDNA was used per well, and we used the following thermocycler conditions: Step 1—95 °C for 10 m, Step 2—95 °C for 15 s, and Step 3—60 °C 45 s. Step 2 to step 3 were repeated a total of 60×. Forward and reverse primers used to perform qPCR for target genes of interest, as well as T_M, can be found in Table S1. Other sets of islets were frozen for RNA extraction to be performed later. Extracted RNA was snap frozen in liquid nitrogen and shipped to Novogene Corporation Inc (Sacramento, CA) for library preparation, RNA sequencing, and bioinformatics analysis. In each case for qPCR and RNAseq, RNA extraction was performed using RNeasy® Micro Kit, with Omniscript RT Kit used to obtain cDNA for qPCR (QIAGEN). Bioinformatics analysis of RNAseq was performed by Novogene Corporation Inc. This included a sample quality control to check for RNA Integrity Number (RIN), with only samples ≥6 further analyzed. After RIN test library preparation was performed, followed by sequencing by synthesis. Once sequence is obtained bioinformatics analysis was performed using FASTQ files to generate Fragments Per Kilobase of exon per Million (FPKM) readcounts. Heat maps were generated using FPKM readcounts, normalized to the FPKM at 2 mM glucose values,

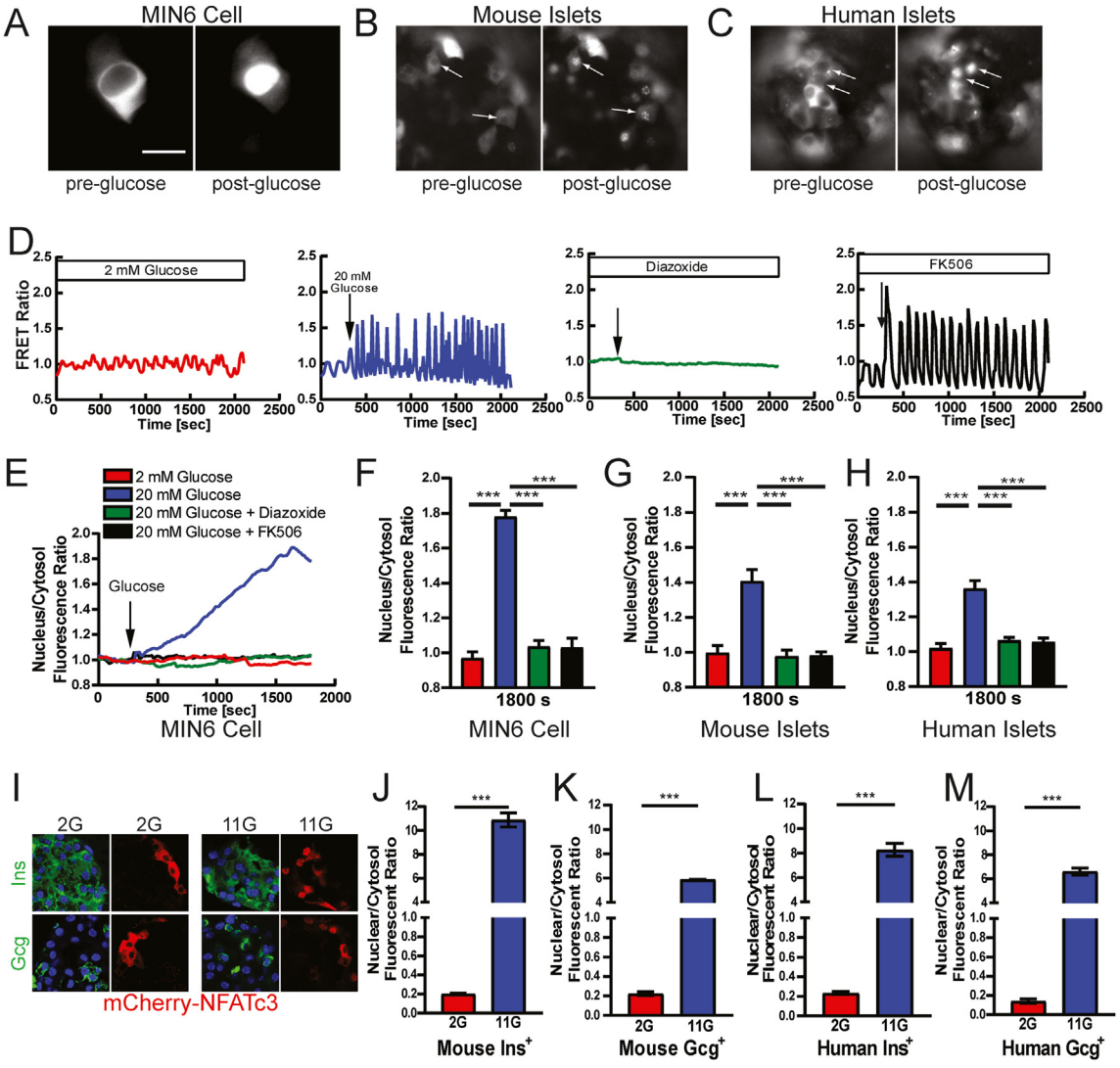

Figure 1: Glucose and membrane potential-dependent activation of NFATc3. A) Image of MIN6 cells transiently transfected with mCherry-NFATc3 at low glucose and 30 min after the addition of high glucose. **B)** As in A for mouse islets virally infected with mCherry-NFATc3. **C)** As in A for human islets from a healthy donor, virally infected with mCherry-NFATc3. **D)** Time-course of FRET ratio from D3cpV Ca^{2+} FRET sensor transfected into MIN6. Ca^{2+} changes were measured under four separate conditions: 2 mM glucose (red), 20 mM glucose (blue), 11 mM glucose + diazoxide (green), and 11 mM glucose + FK506 (black). **E)** NFATc3 translocation to the nucleus in MIN6 cells, for the conditions indicated in D, as measured by the ratio of nuclear to cytoplasmic fluorescence. Traces represent average of all experiments performed in MIN6 cells. **F)** Mean nuclear-cytoplasmic mCherry-NFATc3 ratio 30 min after treatment in MIN6 cells. **G)** As in F for primary mouse islets. **H)** As in F for primary human islets from healthy donors. **I)** Image of insulin or glucagon staining (green) plus mCherry-NFATc3 (red) in mouse islets following incubation with low (2 mM) or high (11 mM) glucose. **J)** Mean nuclear-cytoplasmic mCherry-NFATc3 ratio 30 min after incubation in insulin + cells of mouse islets. **K)** As in J for glucagon + cells of mouse islets. **L)** As in j for insulin + cells of human islets. **M)** As in K for glucagon + cells of human islets. Statistical analysis was done using ANOVA with Tukey HSD post hoc test (F–H) or Student's t-test (J–M). *, **, and *** represent $p = 0.05$, $p = 0.005$, $p = 0.0005$, respectively. Data in F averaged over n = 5,11,8,4 plates respectively (18,31,21,8 cells); data in G averaged over n = 3 mice (12,11,8,9 islets); data in H averaged over n = 6 donors (n = 8 for 2G, 11G + FK506; 28,21,24,33 islets); data in J,K averaged over n = 3 mice, data in L,M averaged over n = 3 donors.

and expressed by taking the log_{10} ($FPKM_{norm}$). Heat map limits were set to *-1* to *+1*.

qPCR was performed to obtain the C_t-value from the target gene and the reference gene by calculating the ΔC_t. This was done by subtracting the target gene from the reference gene (HPRT C_t − Target Gene $C_t = \Delta C_t$). ΔC_t values were normalized to the ΔC_t values for 2-mM glucose treatment.

2.9. In-silico transcription factor binding analysis

Motif enrichment was performed using HOMER [29] version 4.9. The list of predicted NFAT-regulated genes was input into the HOMER script *findMotifs.pl*. This script first identified the regions of DNA in the promoter (300 bp upstream and 50 bp downstream of each gene's TSS). A background set of sequences was then identified based on random sequences from the mm10 genome with matched GC content with the input. The promoter regions and background regions were scanned for known motifs in the HOMER database. A binomial distribution was used to score the enrichment of motifs with respect to the background sequences. Only the significant enrichments were presented, as defined by $p < 0.01$.

Motif finding was performed using fimo from the MEME suite version 5.1.1 [30,31]. First, a mm10 gtf file was downloaded from Ensembl (*wget ftp.ensembl.org/pub/release-96/gtf/mus_musculus/Mus_musculus.GRCm38.96.gtf.gz*) and converted into a bed file using *gtf2bed* from

bedops version 2.4.29 [32] (*awk '{ if ($0 ~ "transcript_id") print $0; else print $0" transcript_id \ "\ ";"; }' Mus_musculus.GRCm38.96.gtf | awk '$3 = = "gene"' | gtf2bed > Mus_musculus.GRCm38.96.bed*). This bed file was modified to include all regions 5000 bp upstream and 5000 bp downstream of the TSS for all predicted NFAT regulated genes using bedtools flank and bedtools slop [33]. The resulting bed file was used to generate a fasta file from the GRCm38 fasta file from Ensembl (*wget ftp://ftp.ensembl.org/pub/release-96/fasta/mus_musculus/dna/Mus_musculus.GRCm38.dna.primary_assembly.fa.gz*) using bedtools *getfasta* [33]. Background sequences were generated using *fasta-get-markov* from the MEME suite using default parameters [30]. Fimo [30,31] from the MEME suite was run using the promoter fasta file, the background fasta file, and motifs downloaded from Jaspar (*http://jaspar.genereg.net/downloads/*).

A custom snakemake pipeline and R scripts to recreate the motif enrichment analysis can be found at *https://github.com/kwells4/benniger_tf_regulators* and will be made available upon publication.

3. RESULTS

3.1. Glucose-dependent electrical changes activate NFATc3 in MIN6 cells, mouse islets, and human islets

To initially modulate electrical activity and measure the activation and translocation of NFATc3, we used the β-cell like mouse insulinoma MIN6 cell line [34]. NFATc3 tagged with GFP was transiently transfected into MIN6 cells, and the ratio of nuclear to cytosolic fluorescence was monitored over time. At low (2 mM) glucose GFP fluorescence was largely localized to the cytoplasm. Upon 20 mM glucose (in combination with 20 mM TEA), there was a substantial increase in nuclear GFP fluorescence indicating NFATc3 activation and translocation to the nucleus (Figure 1A). Similar observations were made in mouse islets and human islets in which NFATc3-GFP was delivered via adenoviral infection: at low (2 mM) glucose GFP fluorescence was largely localized to the cytoplasm whereas upon 11 mM glucose there was a substantial increase in nuclear GFP fluorescence indicating NFATc3 activation (Figure 1B,C). The delivery of mCherry-NFATc3 did not significantly impact cell function, as measured by glucose-stimulated Ca^{2+} dynamics (Figure S1).

As elevated glucose level stimulates membrane depolarization and $[Ca^{2+}]$ elevation, we next tested whether NFATc3 activation that followed elevated glucose level required membrane depolarization. Using a genetically encoded Ca^{2+} probe (D3cpV [35]), Ca^{2+} oscillations were found to be absent at low glucose level; however, as expected, there were robust increases in Ca^{2+} oscillations at elevated (20 mM) glucose (Figure 1D) levels. Upon treatment with the K_{ATP} activator diazoxide, which hyper-polarizes the cell, Ca^{2+} changes were abolished upon elevated glucose levels. In contrast, upon treatment with CaN inhibitor FK506, the Ca^{2+}oscillations at elevated (20 mM) glucose were not perturbed. Using these treatment conditions, we tracked the activation of NFATc3, via its nuclear translocation, over time following glucose elevation. In MIN6 cells, there was a progressive increase in the nuclear localization and activation of NFAT. This elevation was completely absent when maintained at low glucose level (Figure 1E). Similarly, under both diazoxide treatment and FK506 treatment, glucose lacked any activation and nuclear translocation of NFATc3 (Figure 1E), indicating its activation is dependent on increases to the electrical activity. Following quantification, significant nuclear translocation was only observed under elevated glucose, and not under low glucose, upon membrane hyperpolarization with diazoxide, or upon CaN inhibition with FK506 (Figure 1F). Similar observations were also made in primary mouse islets and human islets (Figure 1G,H), where nuclear localization and activation of NFAT was absent under low glucose or elevated glucose levels with either diazoxide treatment or FK506 treatment.

To determine whether glucose-induced nuclear localization and activation of NFATc3 differed between islet β-cells and α-cells, we performed histological analysis of islets post-stimulation with low (2 mM) or elevated (11 mM) glucose (Figure 1I) levels. We observed substantially elevated nuclear localization in both mouse islet β-cells and α-cells following elevated glucose compared to low glucose (Figure 1J,K) level. We observed similar results in human islets (Figure 1L,M). In each case, the level of nuclear localization in α-cells was less than that in β-cells.

NFAT consists of 4-isoforms, with each expressed in a tissue specific manner. All 4 NFAT isoforms are expressed in the β-cell [36,37]. To this end, we tested whether these isoforms were also activated via glucose and electrical activity. In MIN6 cells only NFATc2 and NFATc3 showed robust activation and nuclear translocation upon elevated (20 mM) glucose (Figure S2). No significant nuclear translocation was observed with NFATc1 or NFATc4. Given the fact that in the β-cell high glucose activates both NFATc3 and Erk1/2 and both flank the insulin gene promoter to induce insulin transcription [38], we focused on NFATc3 activation.

The endoplasmic reticulum (ER) is a significant Ca^{2+} store in the cell [39,40], and ER Ca^{2+} release can stimulate insulin secretion [41,42]. As such we tested whether ER Ca^{2+} release is sufficient to stimulate NFATc3 activation. In MIN6 cells, mouse islets and human islets at low glucose thapsigargin-induced ER Ca^{2+} release was sufficient to induce NFATc3 activation and nuclear translocation (Figure S3). Thus, elevated Ca^{2+} resulting from electrical activity and intracellular stores are sufficient to activate NFAT.

3.2. Optogenetic-driven sustained electrical activity activates NFATc3

To further examine the dependence of NFAT activation and translocation on β-cell electrical activity, we used optogenetics. ChR2 is a cationic channel that opens upon blue (450−480 nm wavelength) light, thus depolarizing the cell [43]. When expressed within the β-cell, it allows tight control over the dynamics of electrical activity and $[Ca^{2+}]$, by triggering bursts of action potentials similar to physiological bursts [44,45]. Prior studies have utilized optogenetics to generate different Ca^{2+} waveforms and investigate the link between $[Ca^{2+}]$ dynamics and NFAT activation [46]. Thus, to stimulate islet electrical activity, independent of glucose, we illuminated primary mouse islets with β-cell specific expression of ChR2 [47] with different temporal patterns of light. We first measured the resultant $[Ca^{2+}]$ dynamics following either slow sustained pulses (1.5 min ON/5 min OFF) or more rapid pulses of light (30 s ON/3 m OFF), with an additional intermediate protocol (1 min ON/5 min OFF). In each case, following Rhod-2 staining, pulses of $[Ca^{2+}]$ were generated closely matching the pulse stimulation protocol (Figures 2A,B and S4A,B). Furthermore, similar amplitudes were reached such that the time averaged $[Ca^{2+}]$ was similar across all three protocols (Figures 2C and S4C). We next examined the resultant activation of NFAT through measuring the coincident translocation of mcherry-NFATc3 (Figure 2D), where use of mCherry avoids spectral cross-talk with the ChR2-YFP tag [48]. Upon the slowest protocol there was a progressive elevation in NFAT activation and nuclear translocation following each sustained pulse of $[Ca^{2+}]$ elevation (Figure 2D,E). In contrast the more rapid pulse protocols did not elicit any NFAT activation and nuclear translocation (Figures 2F and S4D,E). As such, only the slow pulse protocol generated any significant NFAT activation and nuclear translocation

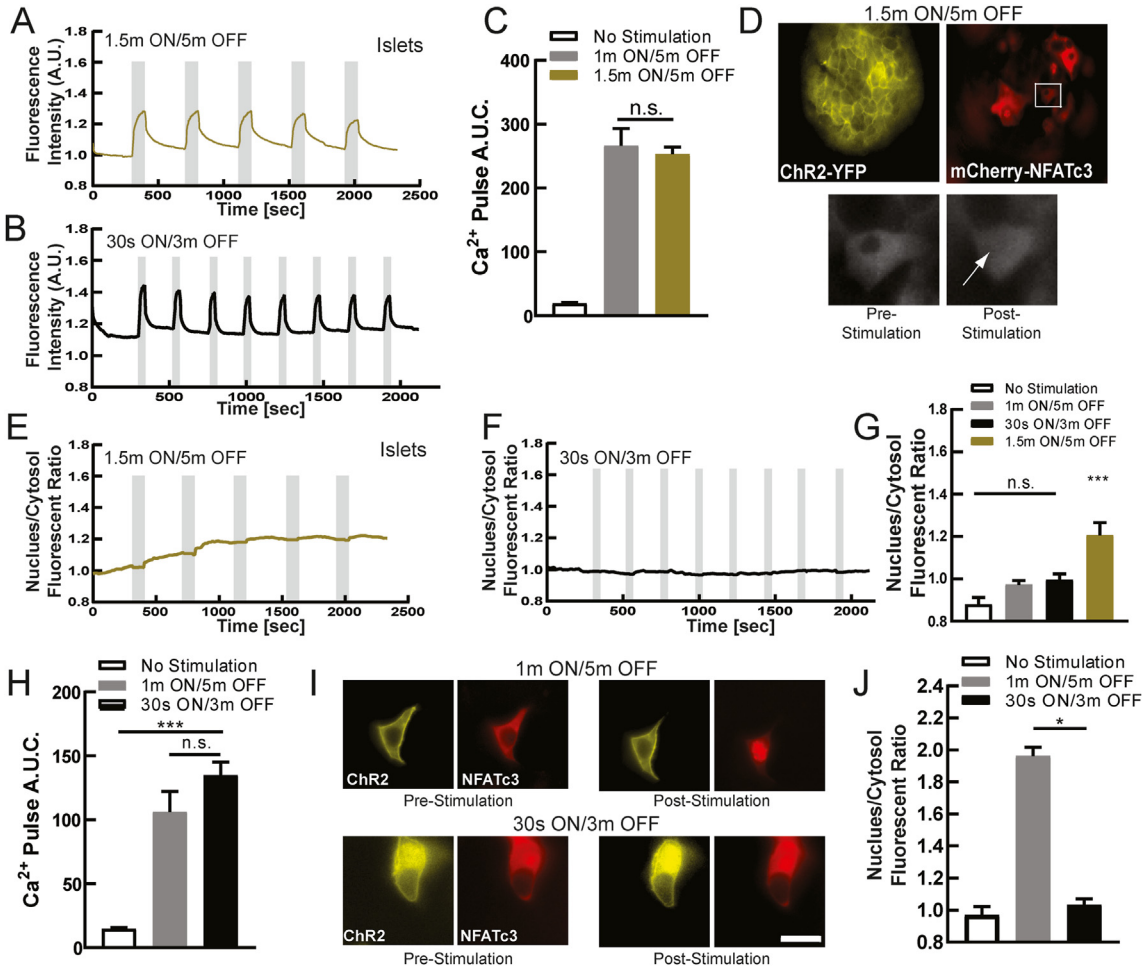

Figure 2: Dynamic Ca^{2+} changes via optogenetics activates NFATc3. **A)** Mean Ca^{2+} changes in mouse islets expressing ChR2(H134R) in the beta-cell, at 2 mM glucose following 1.5 min ON/5 min OFF optical stimulation protocol. Grey indicates duration of optical stimulation. **B)** As in A for 30 s ON/3 min OFF optical stimulation protocol. **C)** Area under the curve (AUC) for each stimulation pulse protocol, as well as time course lacking stimulation. **D)** Representative images of ChR2-expressing islet infected with mCherry-NFATc3, demonstrating NFATc3 translocation following optical stimulation (1.5 min ON/5 min OFF). **E)** Mean time-course of mCherry-NFATc3 nucleus/cytosol fluorescent ratio following the 1.5 min ON/5 min OFF optical stimulation pulse protocol. **F)** As in E for the 30 s ON/3m OFF protocol. **G)** Mean nuclear-cytoplasmic mCherry-NFATc3 ratio 30 min after optical stimulation. **H)** Area under the curve (AUC) of Ca^{2+} changes for stimulation pulse protocols (1 min ON/5 min OFF or the 30 s ON/3 min OFF), as well as time-course lacking stimulation, in MIN6 cells transfected with ChR2. **I)** Representative images of ChR2-expresisng MIN6 cell transfected with mCherry-NFATc3, demonstrating NFATc3 translocation following optical stimulation. **J)** Mean nuclear-cytoplasmic mCherry-NFATc3 ratio 30 min after optical stimulation in MIB6 cells. Statistical analysis was done using ANOVA with Tukey HSD post hoc test. *, **, and *** represent $p = 0.05$, $p = 0.005$, $p = 0.0005$, respectively. Data in C averaged over $n = 4$ mice ($n = 6$ for 1.5 min/5 min; 15,28 islets); data in G averaged over $n = 4$ mice ($n = 6$ for 1m/5m; 13,15 islets); data in H averaged over $n = 10,12$ plates (29,27 cells); data in J averaged over $n = 10,24$ plates (30,55 cells).

compared to in the absence of ChR2 stimulation (Figures 2G and S4F). Interestingly, this slower protocol most closely matches physiologically slow Ca^{2+} oscillatory dynamics within the islet under elevated glucose [5] These data demonstrate that the physiological pulsatile [Ca^{2+}] dynamics is critical to activate NFATc3 in the β-cell.

We further examined the link between [Ca^{2+}] dynamics and NFATc3 activation in the β-cell using MIN6 cells transiently transfected with ChR2-YFP. Following Rhod2-AM staining, similar [Ca^{2+}] dynamics were elicited by each pulse protocol (Figure S4G,H), as in primary islets. For the intermediate (1m ON/5m OFF) and fast (30s ON/3m OFF) protocols, similar amplitudes were reached. As such, the time averaged [Ca^{2+}] was similar across both protocols (Figure 2H). We were unable to utilize the slowest pulse protocol (1.5m ON/5m OFF) owing to the slower Ca^{2+} extrusion in MIN6 cells. In cells co-transfected with mCherry-NFATc3 we again examined the resultant activation and translocation of NFAT. During the slower intermediate protocol there was a progressive elevation in NFAT activation and nuclear translocation following each sustained pulse of [Ca^{2+}] elevation (Figures 2I and S4I). In contrast the more rapid fast pulse protocol did not elicit any NFAT activation and nuclear translocation (Figure S4J). As such only the slower intermediate pulse protocol generated any significant NFAT activation and nuclear translocation compared to in the absence of ChR2 stimulation (Figure 2J). Thus, a similar importance for pulsatile Ca^{2+} dynamics and NFATc3 activation were found in MIN6 cells, albeit with a shift in frequency dependence compared to primary islets.

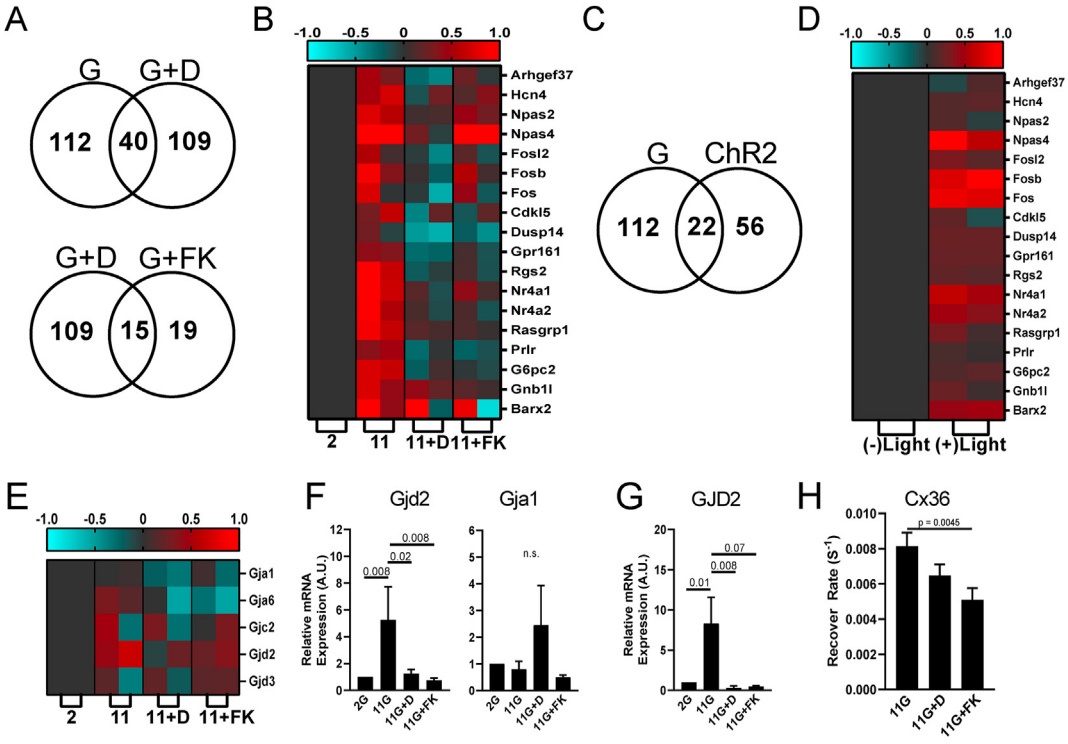

Figure 3: Acute gene transcription changes following elevated electrical activity. A) Venn diagram showing numbers of genes that are differentially expressed between glucose stimulation and application of K_{ATP} opener diazoxide upon glucose stimulation (upper) or between diazoxide application and FK506 application, upon glucose stimulation (lower), each in mouse islets. **B)** Heat map depicting genes previously identified to regulate beta-cell proliferation and insulin secretion, following stimuli applied in A. Displayed is the subset of genes that shows the highest expression changes across the stimuli applied. **C)** Venn diagram showing numbers of genes that are differentially expressed between glucose stimulation and ChR2 optical stimulation in mouse islets. **D)** Heat map depicting genes identified in B, following stimuli applied in C. **E)** Heat map depicting connexin genes, following stimuli applied in A. **F)** qPCR of Gjd2 (Cx36) and Gja1 (Cx43) expression in mouse islets, following stimuli applied in A. **G)** qPCR of GJD2 (Cx36) expression in human islets, following stimuli applied in A. **H)** Fluorescence recovery after photobleaching measurements of gap junction permeability. Shown are data collected in islets treated with elevated glucose level alone or upon diazoxide. Statistical analysis was done using ANOVA with Tukey HSD post hoc test. p values are indicated. 'n.s.' refers to $p > 0.2$. RNAseq data in A-E represented from 2 independent experiments. Data in F averaged over $n = 5$ experiments; data in G averaged over $n = 6$ (correct) experiments; data in H averaged over $n = 8$ experiments.

3.3. Altered electrical activity regulates RNA gene transcription of mouse islets

Thus far, we have demonstrated that glucose stimulates NFAT activation and nuclear translocation, and this strictly requires elevated electrical activity. Furthermore, the physiological dynamics of electrical activity is critical to generate sustained [Ca^{2+}] elevation required for NFAT activation and translocation. NFAT regulates many genes critical for β-cell function and proliferation [49,50] and we next examined whether elevated electrical activity is important for NFAT-regulated gene expression. We incubated islets with either low or high glucose, as well as high glucose plus diazoxide to inhibit electrical activity or FK506 to inhibit CaN-NFAT signaling. Following 4 h, we isolated RNA to examine rapidly activated genes more likely to represent direct targets. In neurons, NFAT target gene expression can elevate 4–5 h following depolarization-induced NFAT activation and translocation [51]. We observed 57 genes were significantly upregulated by glucose and 55 genes significantly downregulated by glucose. Compared to these 112 glucose-regulated genes, 109 showed a significant reversal in gene expression upon diazoxide treatment. 40 of these genes showed overlap between the two conditions, indicating their dependence on electrical activity. Of the 109 genes that showed a significant reversal in gene expression upon diazoxide treatment 19 showed a significant reversal in gene expression upon FK506 treatment, indicating their dependence on CaN-NFAT activity (Figures 3A and S4). We next identified a subset of genes that have previously been associated with β-cell function and proliferation. These included immediate early genes such as the Fos family of genes, as well as Cdkl5, Dusp14, and Gpr161 genes [49] or Npas4 which is known to have cytoprotective properties in β-cells [15]. Of these 18 genes that show the most significant increase in expression with elevated glucose and decrease in expression with glucose plus diazoxide, all but one also showed significant decrease in expression with FK506 (Figure 3B). We performed *in silico* motif analysis of those genes that showed overlap in expression changes upon glucose or glucose plus diazoxide treatments. We observed a significant enrichment of NFAT binding motifs in these genes ($p = 0.0012$), consistent with a significant subset of genes showing regulation dependent on CaN-NFAT activity (Figure S5). We also observed enrichment of binding motifs for other β-cell enriched transcription factors such as Nkx6.1. Thus many 'excitability-regulated' genes that have a functional role in the β-cell are regulated by CaN-NFAT signaling. We also observed enrichment of Mef2b ($p = 0.0044$), but not of other Ca^{2+}-regulated transcription factors (e.g. CREB5, $p = 0.032$; NeuroD, $p = 0.46$; with $p < 0.01$ the threshold for significance). This indicates that some of the 'excitability-regulated' genes are likely regulated by other Ca^{2+}-regulated transcription factors.

We next performed analogous transcription measurements in islets expressing ChR2 in the β-cell. Following 4 h of pulsatile light stimulation

(1.5 min ON/5 min OFF, Figure 2A), we again isolated RNA to examine genes activated rapidly by elevated electrical activity independent of glucose. We observed 25 and 31 genes that were significantly upregulated or downregulated, respectively, following ChR2 stimulation. Of these 56 ChR2-regulated genes, 22 were also observed to show glucose-regulated expression (Figure 3C). Similarly, of those genes with roles in the β-cell that most significantly changed upon glucose/diazoxide treatment, the vast majority also showed upregulation with ChR2 stimulation (Figure 3D). Thus, there are several genes in which RNA levels are altered in response to changes to the electrical activity of the β-cell, dependent on CaN-NFAT signaling.

GJD2 encodes Connexin-36 (Cx36) which forms gap junction channels that electrically couple β-cells within the islets and coordinate Ca^{2+} regulation and insulin release across the islet [52]. While not among the genes most highly upregulated by glucose, we observed that *GJD2* expression significantly increased upon glucose elevation, which was reversed by both diazoxide and FK506, (Figure 3E) indicating another gene in which expression is rapidly regulated by electrical activity and CaN-NFAT signaling. No other gap junction gene expressed within the islet showed such regulation. qPCR analysis supported these findings indicating glucose elevates *GJD2* expression (encoding Cx36) which is reversed by diazoxide and FK506, whereas *GJA1* (encoding Cx43), the other major connexin expressed within the islet, shows no such regulation (Figure 3F). We also observed similar regulation of *GJD2* expression in human islets (Figure 3G), where *GJD2* is highly enriched in human β-cells, as in mouse β-cells (Figure S6) [53—56]. Following 24h culture at elevated glucose, both diazoxide and FK506 significantly reduced functional gap junction permeability within the islet [57] (Figure 3H). Thus, the elevation in *GJD2* expression following glucose-stimulated electrical activity and CaN-NFAT signaling is functionally relevant.

A previous work has established that several genes involved in islet function and islet development/proliferation are regulated by CaN-NFAT signaling. RNAseq analysis or qPCR analysis (Figure S7) each showed that these genes were not robustly increased acutely by elevated glucose nor decreased by diazoxide or FK506 treatment. An exception was that both FoxM1 and Hnf4α both showed significant changes in expression under elevated glucose which recovered upon diazoxide or FK506 treatment, indicating these genes may be acutely regulated by elevated electrical activity. Similarly, the NFAT subunits themselves also showed little acute changes in gene expression under these conditions (Figure S7). Thus, even though several genes important to β-cell function and development are acutely regulated by electrical activity and CaN-NFAT signaling, these are distinct from those identified in prior studies to be chronically regulated by CaN-NFAT signaling.

3.4. Decline and restoration of NFATc3 activation in diabetic islets

Diabetic conditions disrupt $[Ca^{2+}]$ in β-cells. This includes altered ER Ca^{2+} handling [58], membrane excitability [59], and gap junction communication [9,60], thus disrupting the dynamics of $[Ca^{2+}]$. To test if NFATc3 is altered under diabetic conditions, we first applied proinflammatory cytokines, which are elevated during diabetes, acutely to transduced mouse and human islets. Treatment with proinflammatory cytokines disrupts $[Ca^{2+}]$ elevation and dynamics [9,61,62]. Following 2 h incubation with proinflammatory cytokines, in primary mouse islets NFATc3 activation and translocation were blunted compared to untreated islets (Figure 4A,B). Similar blunting to NFATc3 activation and translocation was observed in primary human islets treated with proinflammatory cytokines (Figure 4C), and in MIN6 cells treated with proinflammatory cytokines (Figure S8A,B). Therefore, under acute diabetogenic condition NFAT activation is dysregulated in the β-cell.

To test whether NFATc3 is dysregulated in more chronic cases of diabetes, we examined human islets obtained from either healthy donors or those with T2D. Human islets from donors with T2D showed diminished $[Ca^{2+}]$ under elevated glucose levels but retained robust KCl-stimulated $[Ca^{2+}]$ (Figure S9A). Under low levels of glucose NFATc3 showed little activation and translocation in human islets from both healthy donors and T2D donors (Figure 4D). Under elevated glucose progressively elevated activation and translocation NFATc3 occurred in human islets from healthy donors (as already presented, Figure 1). However, in human islets from T2D donors little NFATc3 activation and translocation was observed (Figure 4D). Over several donors, significant NFAT activation was observed in healthy donor islets but not in T2D donor islets (Figure 4E). Specifically, human islets from 5/6 healthy donors showed NFAT activation and translocation under elevated glucose, whereas human islets from only 1/7 donors with T2D showed NFAT activation and translocation under elevated glucose. Thus, NFAT activation is significantly diminished in human T2D, which well correlates with the lack of robust glucose-stimulated $[Ca^{2+}]$ elevation.

To further test whether diminished NFAT activation and translocation in human T2D result from diminished glucose-stimulated $[Ca^{2+}]$ elevation, we applied pharmacological stimulation of electrical activity and Ca^{2+} influx. Both the K_{ATP} channel inhibitor glibenclamide and voltage gated Ca^{2+} channel activator quercetin elevated $[Ca^{2+}]$ in human T2D islets (Figure S9B,C) indicating that the blunted glucose-stimulated $[Ca^{2+}]$ likely resulted from diminished glucose-sensing. We next tested whether these treatments would restore NFAT activation in T2D islets. Under elevated glucose, glibenclamide and quercetin led to progressively elevated activation and translocation of NFATc3 (Figure 4F—I). Among several donors, significant NFAT activation was observed under both glibenclamide and quercetin, compared to elevated glucose alone, with quercetin eliciting a greater activation and translocation of NFATc3 (Figure 4J). These results show that islets from T2D donors are electrically dysfunctional, as has been previously observed [59,63], and this diminishes $[Ca^{2+}]$ elevation and NFAT activation. However, pharmacological agents that increase electrical activity to elevate $[Ca^{2+}]$ can restore the activation of NFATc3.

4. DISCUSSION

Nuclear factor of activated T-cell (NFAT) is important for many tissues, playing a key role in linking cell activation to gene expression and cell remodeling. Within the islet, NFAT regulates many genes involved in β-cell function, particularly in glucose sensing and insulin granule biogenesis [16,21]. NFAT is also a critical factor in β-cell proliferation, with inhibition of NFAT dephosphorylation and deactivation stimulating β-cell proliferation, including in human β-cells [64]. While NFAT is activated under elevated glucose, little additional information is available for how NFAT is activated within the β-cell. Given the importance for electrical activity and Ca^{2+} influx in the β-cell, and the role for $[Ca^{2+}]$ elevation to activate NFAT in other systems, we sought to determine the link between the electrical activity of the β-cell and NFAT activation and downstream gene expression and how this is perturbed in diabetes when electrical activity is disrupted.

4.1. Dynamic β-cell electrical activity regulates NFAT activation

We demonstrated that elevated electrical activity and $[Ca^{2+}]$ were required for NFAT activation. Upon membrane hyper-polarization,

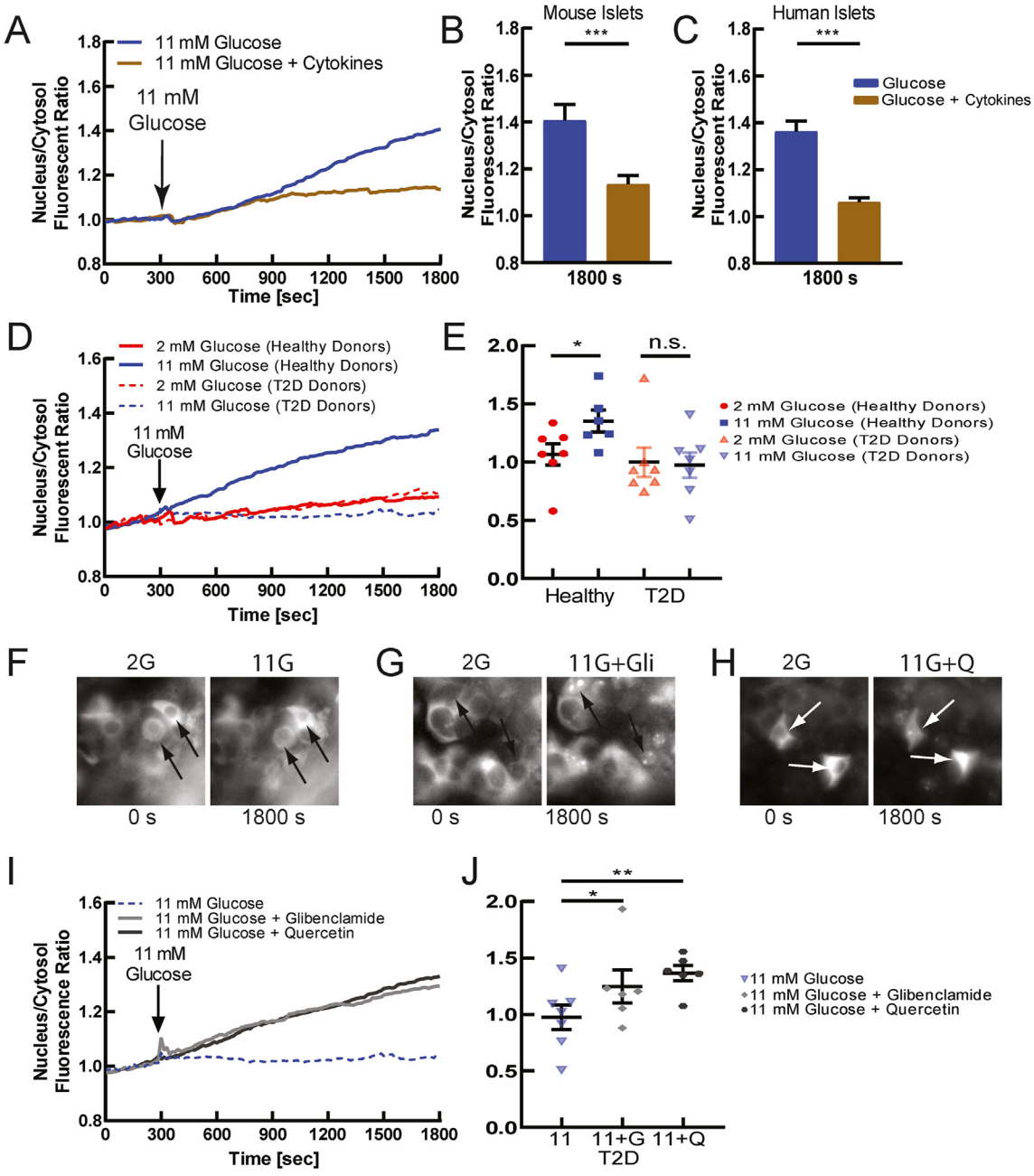

Figure 4: NFATc3 activation is diminished in diabetes due to diminished electrical activity. A) Mean NFATc3 nuclear translocation over time, as measured by the ratio of nuclear to cytoplasmic fluorescence of mCherry-NFATc3, in untreated (blue) or cytokine-treated (brown) mouse islets, following elevated glucose. Cytokine treatment contains 0.005 μg/mL IL1-β, 0.01 μg/mL TNF-α, and 0.1 μg/mL IFN-γ for 2 h in DMEM or RPMI-1640 media. **B)** Mean nuclear-cytoplasmic mCherry-NFATc3 ratio 30 min after treatment in mouse islets, as in A. **C)** As in B for human islets from healthy donor treated with proinflammatory cytokines. **D)** Mean NFATc3 nuclear translocation over time measured in human islets from healthy donors and donors with T2D, at 2 mM glucose or following stimulation with 11 mM glucose. **E)** Nuclear-cytoplasmic mCherry-NFATc3 ratio 30 min after treatment in human islets, as in A. Each dot represents the average all cells and islets from a specific healthy donor or donor with T2D. **F)** Representative images of mCherry-NFATc3-infected human islet under low (2 mM) and high (11 mM) glucose. **G)** As in F under-elevated (11 mM) glucose or elevated glucose levels with glibenclamide (Glib). **H)** As in F under-elevated (11 mM) glucose or elevated glucose with Quercetin (Q). **I)** Mean NFATc3 nuclear translocation over time, under elevated glucose alone or including glibenclamide (Glib) or quercetin (Q). **J)** Mean nuclear-cytoplasmic mCherry-NFATc3 ratio 30 min after treatments in F—H. Each dot represents the average over all cells and islets from a specific donor with T2D, treated with the agents indicated. Statistical analysis was done using ANOVA with Tukey HSD post hoc test. *, **, and *** represent $p = 0.05$, $p = 0.005$, $p = 0.0005$, respectively and n.s. means no significance. Data in B averaged over $n = 3$ mice (12 islets); data in C averaged over $n = 8$ donors (30 islets); data in E representative of $n = 6$ healthy donors (21 islets) and $n = 7$ donors with T2D (28 islets); data in J representative of $n = 6$ donors with T2D (11,11,12 islets).

NFAT activation by glucose was completely abolished across all models examined (Figure 1). Furthermore, increased electrical activity was sufficient to activate NFAT, as demonstrated upon ChR2 stimulation at low glucose. While Ca^{2+} is long-known to activate NFAT, and elevated glucose in the β-cell is known to activate NFAT, this central role for β-cell electrical activity was previously not established.

Importantly, we observed this dependence on electrical activity only for c2 and c3 subunits, where the c2 subunit has also been linked to multiple aspects of β-cell function [16,21].

Unexpectedly, we also demonstrated that the dynamics of electrical activity and [Ca^{2+}] are important for NFAT activation: only slow sustained oscillations in [Ca^{2+}] were sufficient for NFAT activation in both primary mouse islets and MIN6 cells (Figure 2). This was independent of Ca^{2+} 'dose' as similar time-averaged [Ca^{2+}] was observed. This frequency-dependence is surprising as in chemical synapses NFAT lacks significant frequency dependence (as opposed to CaMKII for example) [51]. However, in chemical synapses, the frequency varies with much faster time scales (seconds), that the time-scale within the islet (minutes). By using synthetic biology approaches in HeLa cells, NFAT showed greater dependence on duty cycle than oscillation frequency [46], also not consistent with our results. Nevertheless, [Ca^{2+}] oscillations are more effective at inducing gene expression in T cells via NFAT compared to steady state levels [65], indicating some frequency dependence to NFAT. The origin of the frequency dependence that we observe within the β-cell remains unclear. We speculate that it may originate from either some cooperativity that may only present on a minute time-scale, or that NFAT rephosphorylation and deactivation is negatively regulated by Ca^{2+}-dependent processes. Determining these mechanisms will be important. Furthermore, while ChR2 stimulation induces action potential bursts that resemble physiological bursts [44], we cannot exclude that differences may have an impact. For example, the inward cation current that results from ChR2 activation will differ from the decrease in outward current that results from glucose metabolism and K_{ATP} closure, thus impacting the AP shape and burst duration, as well as the plateau potential. Nevertheless, in revealing this unexpected frequency dependence, the use of optogenetics was critical, and this reveals a new avenue for optogenetic approaches.

The glucose-activation of NFAT was also diminished under diabetic conditions (Figure 4). Likely, this was a result of diminished [Ca^{2+}] we measured, as pharmacological elevation of [Ca^{2+}] via K_{ATP} inhibition or Ca_V stimulation recovered NFAT activation. We and other groups have measured diminished [Ca^{2+}] in multiple models of diabetes, with this disruption originating from altered glucose-sensing and mitochondrial dysfunction [9,52,66]. However, [Ca^{2+}] oscillations are also disrupted in models of diabetes, showing shorter pulse duration [67]. Thus, given elevated [Ca^{2+}] does still exist in diabetic islets, another possibility is that the altered frequency and pulse duration is impacting NFAT activation in diabetes. Irrespective of the precise cause, the dysregulated [Ca^{2+}] in diabetes is diminishing NFAT activation, as such factors that can promote robust elevated [Ca^{2+}] will be important to recover NFAT activation and downstream transcriptional regulation.

4.2. NFAT links cell activity with gene expression

We observed that several genes were upregulated or downregulated by conditions that increase electrical activity and [Ca^{2+}] within the islet: both under glucose stimulation where up/downregulation was reversed by diazoxide-induced K_{ATP} opening; as well as following dynamic ChR2 stimulation (Figure 3). Many of the genes we identified were different from those previously identified to be NFAT regulated following genetic manipulation, including NFATc2 overexpression or CaN knockout [16,21,68]. Further, the genes we identified also showed differences from those following CaN inhibition in mouse islets or human islets [69]. The genes we identified included Ca^{2+} regulated genes that have been identified in other systems, such as Npas and Fos family [70—73]. These genes are important to pathways underlying β-cell secretion, cytoprotection, and proliferation [15,50]. The genes we identified also included those associated with cell cycle regulation and proliferation, consistent with the role for NFAT to regulate β-cell proliferation.

The difference between the specific CaN-NFAT-regulated genes identified in this study, and those identified in prior studies, may result from the time-course of action. We examined genes rapidly upregulated by [Ca^{2+}] on a ∼4-h timescale. Prior studies have utilized overexpression systems or gene knockouts that reveal longer-term regulation or have used longer time-scales for culture with CaN inhibitors. Thus, other transcription factors regulated by NFAT may be impacting these previously identified CaN-NFAT-regulated genes within the islet. Alternatively given that CaN is an effector for other molecules beyond NFAT, we may not be observing solely CaN-NFAT regulation. Nevertheless, we still do not see strong concordance between our gene expression results following short-term pharmacological inhibition of FK506 and prior genetic knockout of CaN [21] or longer-term CaN inhibition [69]: For example we do not observe changes in genes associated with insulin granule biogenesis and exocytosis or genes associated with proliferation that have been observed in other studies. This suggests that the different time-scales being examined is the more likely explanation between the lack of correspondence between our study and prior results. Nevertheless, recent studies have identified the nuclear receptor Nr4a1 as critical for NFATc2-regulation of β-cell proliferation [74]. We identified this gene to be acutely regulated by electrical activity, Ca^{2+} elevation, and CaN-NFAT signaling (Figure 3). As such, some genes do show similarities across timescales.

Despite the short timescales used, the gene expression changes were not necessarily directly regulated by CaN-NFAT signaling. Other Ca^{2+}-regulated transcription factors may also be involved. For example, NFAT binding sites are present in the promoter region of Npas4 (Figure S5). Our *in silico* analysis did show an enrichment of NFAT binding sites in the gene promoters we identified to be regulated by excitability (Figure S7); supporting a direct role for CaN-NFAT signaling in a large proportion of these genes. However, we did also identify an enrichment of Mef2b binding sites, indicating the direct role of other Ca^{2+}-regulated transcription factors in some of these genes.

Some gene expression difference was found between those genes upregulated by elevated glucose level that reversed upon hyperpolarization by diazoxide but lack upregulation by ChR2 stimulation. These differences may reflect an additional requirement of electrical activity, Ca^{2+} elevation and CaN-NFAT signaling, but also glucose acting via other pathways. Given the activation of NFAT by thapsigargin, we would also expect similar changes to gene expression as under ChR2 stimulation. However, the induction of ER stress due to ER Ca^{2+} depletion may have a further impact on gene expression.

Indeed, when electrical activity and Ca^{2+} remain chronically suppressed via K_{ATP} mutation, islets show differing functional properties beyond electrical activity, even when the secondary effects of chronic hyperglycemia are factored out [75]. Similarly, if [Ca^{2+}] remains chronically elevated, also via K_{ATP} mutation, numerous transcriptional changes occur [76]. Pharmacologically-altered electrical activity impacts NFAT activation and downstream gene expression. Therefore, the altered electrical activity and NFAT activation in diabetes will likely impact downstream, gene expression, and may underlie further islet dysfunction and diabetes progression. As such, restoring normal electrical activity may have a broader impact beyond stimulating insulin release.

4.3. Activity-dependent regulation of Cx36

Among the genes upregulated by elevated glucose level and down regulated by membrane hyperpolarization induced by diazoxide was *GJD2*, which encodes Cx36 and forms gap junction channels within the

islet (Figure 3F–H). Thus, increased glucose level enhances gap junction coupling, at least in part by electrical activity and Ca^{2+} influx. This is supported by functional data in which increased gap junction permeability was decreased by either membrane hyperpolarization or FK506-inhibition of CaN-NFAT signaling. Gap junction permeability and conductance are also enhanced following elevated glucose level at much shorter time scales (e.g. <1h) than the time-scale on which we observed enhanced *GJD2* expression (>4h) [57,77]. Thus, while elevated glucose level may stimulate increased *GJD2* transcription via elevated [Ca^{2+}] and CaN-NFAT, glucose may also be required for post-translational regulation such as enhancing channel trafficking. Importantly, and as discussed above, it is unclear whether NFAT directly binds to the *GJD2* gene and thus whether NFAT signaling directly regulates *GJD2* expression. For example we measure a decrease in the expression of the Ca^{2+}-regulated transcription factor Npas4 upon FK506-inhibition of CaN-NFAT signaling (Figure 3B), where Npas4 can bind to the *GJD2* gene [78]. Thus, detailed analysis of the transcription factors that link cell excitability and Ca^{2+} with *GJD2* expression will be needed in future work.

Cx36 gap junction coupling is critical for the function of mouse islets [79,80]; however, and it has been under studied in human islets. *GJD2* is enriched in human β-cells as in mouse β-cells. We also observed similar regulation of *GJD2* expression by membrane potential and CaN-NFAT signaling in the human islet (Figure 3G). However, it will be important to fully establish the role Cx36 gap junction coupling plays in the human islet before speculating how electrical activity-dependent gap junction coupling may impact human islet function.

The electrical activity-dependent gap junction coupling that we observe may be important in the context of islet function: at elevated glucose, our results imply that increased electrical activity and [Ca^{2+}] would lead to rapidly enhanced gap junction electrical coupling. In the context of cellular heterogeneity, this would ensure those more excitable cells with increased electrical activity and [Ca^{2+}] would develop increased electrical coupling. A key role of electrical coupling is to coordinate different responses between cells [52,81]. As such, we speculate that an increase in electrical coupling would increase the integration of the cell with the rest of the islet and thus overcome heterogeneous responses. For example, if a cell transitioned to become more proliferatively competent or entered the cell cycle, its glucose responsiveness and insulin-secretory capacity would likely decline [56,82]. We speculate that this may reduce electrical coupling in the less glucose-responsive cells, as has been observed for some cell subpopulations [59]. This reduced electrical coupling would prevent the less-responsive cell negatively impacting the glucose responsiveness of the rest of the islet. Therefore, the activity-dependent regulation of Cx36 gap junction coupling within the islet may impact how functionally heterogeneous cells within the islet respond to dynamic changes in heterogeneity.

4.4. Conclusions

In summary, here we demonstrate that the electrical activity of the β-cell is critical for the activation of NFAT, its nuclear translocation, and downstream gene transcription, particularly for a set of Ca^{2+} activated genes and other NFAT-regulated genes. This includes *GJD2* and the formation of Cx36 gap junction channels. The dysregulated electrical activity and [Ca^{2+}] in diabetes lead to diminished or absent glucose-regulated NFAT activation, which can be rescued by pharmacological stimulation of electrical activity. This knowledge will be important to understand the regulation of NFAT and its target genes under normal and pathophysiological conditions.

DATA AVAILABILITY

All data presented in this study are available upon request.

ACKNOWLEDGEMENTS

We would like to thank the Islet Isolation Core Facility at the Barbara Davis Center for Diabetes for allowing us to perform pancreatic mouse isolation and digestion to obtain islets. We would also like to thank Dr. Mark Dell'Aqua in the Department of Pharmacology at the University of Colorado Anschutz Medical Campus for giving us the fluorescent-protein-tagged NFATc3 constructs. RKPB has received support from NIH grants R01 DK102950, R01 DK106412, and JDRF grants 1-INO-2017-435-A-N. DGR has received support from NIH grant F31 DK121488. Microscopy use was supported in part by NIH grant P30 DK116073 and the University of Colorado Neurotechnology center. The funders had no role in study design, data collection and analysis, decision to publish, or preparation of the manuscript.

CONFLICT OF INTEREST

All authors declare that no competing interests exist.

APPENDIX A. SUPPLEMENTARY DATA

Supplementary data to this article can be found online at https://doi.org/10.1016/j.molmet.2021.101430.

REFERENCES

[1] Arkhammar, P., Nilsson, T., Rorsman, P., Berggren, P.O., 1987. Inhibition of ATP-regulated K+ channels precedes depolarization-induced increase in cytoplasmic free Ca2+ concentration in pancreatic beta-cells. Journal of Biological Chemistry 262(12):5448–5454.

[2] Ashcroft, F.M., Harrison, D.E., Ashcroft, S.J., 1984. Glucose induces closure of single potassium channels in isolated rat pancreatic beta-cells. Nature 312(5993):446–448.

[3] Cook, D.L., Satin, L.S., Ashford, M.L., Hales, C.N., 1988. ATP-sensitive K+ channels in pancreatic beta-cells. Spare-channel hypothesis. Diabetes 37(5): 495–498.

[4] Notary, A.M., Westacott, M.J., Hraha, T.H., Pozzoli, M., Benninger, R.K., 2016. Decreases in gap junction coupling recovers Ca2+ and insulin secretion in neonatal diabetes mellitus, dependent on beta cell heterogeneity and noise. PLoS Computational Biology 12(9):e1005116.

[5] Satin, L.S., 2000. Localized calcium influx in pancreatic beta-cells: its significance for Ca2+-dependent insulin secretion from the islets of Langerhans. Endocrine 13(3):251–262.

[6] Hellman, B., 2009. Pulsatility of insulin release–a clinically important phenomenon. Upsala Journal of Medical Sciences 114(4):193–205.

[7] Meier, J.J., Veldhuis, J.D., Butler, P.C., 2005. Pulsatile insulin secretion dictates systemic insulin delivery by regulating hepatic insulin extraction in humans. Diabetes 54(6):1649–1656.

[8] Rupnik, M., 2009. All together now: exocytose or fail. Islets 1(1):78–80.

[9] Farnsworth, N.L., Walter, R.L., Hemmati, A., Westacott, M.J., Benninger, R.K., 2016. Low level pro-inflammatory cytokines decrease Connexin36 gap junction coupling in mouse and human islets through nitric oxide-mediated protein kinase cdelta. Journal of Biological Chemistry 291(7):3184–3196.

[10] Rasmussen, H., Jensen, P., Lake, W., Goodman, D.B., 1976. Calcium ion as second messenger. Clinical Endocrinology 5(Suppl):11S–27S.

[11] Dalle, S., Quoyer, J., Varin, E., Costes, S., 2011. Roles and regulation of the transcription factor CREB in pancreatic beta -cells. Current Molecular Pharmacology 4(3):187–195.

[12] Persaud, S.J., Liu, B., Sampaio, H.B., Jones, P.M., Muller, D.S., 2011. Calcium/calmodulin-dependent kinase IV controls glucose-induced Irs2 expression in mouse beta cells via activation of cAMP response element-binding protein. Diabetologia 54(5):1109—1120.

[13] Sabatini, P.V., Speckmann, T., Lynn, F.C., 2019. Friend and foe: beta-cell Ca(2+) signaling and the development of diabetes. Molecular Metabolism 21:1—12.

[14] Schofl, C., Waring, M., Bergwitz, C., Arseniev, L., von zur Muhlen, A., Brabant, G., 2002. Cyclic-adenosine 3',5'-monophosphate-stimulated c-fos gene transcription involves distinct calcium pathways in single beta-cells. Molecular and Cellular Endocrinology 186(1):121—131.

[15] Speckmann, T., Sabatini, P.V., Nian, C., Smith, R.G., Lynn, F.C., 2016. Npas4 transcription factor expression is regulated by calcium signaling pathways and prevents tacrolimus-induced cytotoxicity in pancreatic beta cells. Journal of Biological Chemistry 291(6):2682—2695.

[16] Heit, J.J., Apelqvist, A.A., Gu, X., Winslow, M.M., Neilson, J.R., Crabtree, G.R., et al., 2006. Calcineurin/NFAT signalling regulates pancreatic beta-cell growth and function. Nature 443(7109):345—349.

[17] Lawrence, M.C., Bhatt, H.S., Easom, R.A., 2002. NFAT regulates insulin gene promoter activity in response to synergistic pathways induced by glucose and glucagon-like peptide-1. Diabetes 51(3):691—698.

[18] Lawrence, M.C., Bhatt, H.S., Watterson, J.M., Easom, R.A., 2001. Regulation of insulin gene transcription by a Ca(2+)-responsive pathway involving calcineurin and nuclear factor of activated T cells. Molecular Endocrinology 15(10):1758—1767.

[19] Redmon, J.B., Olson, L.K., Armstrong, M.B., Greene, M.J., Robertson, R.P., 1996. Effects of tacrolimus (FK506) on human insulin gene expression, insulin mRNA levels, and insulin secretion in HIT-T15 cells. Journal of Clinical Investigation 98(12):2786—2793.

[20] Nguyen, T., Di Giovanni, S., 2008. NFAT signaling in neural development and axon growth. International Journal of Developmental Neuroscience 26(2):141—145.

[21] Goodyer, W.R., Gu, X., Liu, Y., Bottino, R., Crabtree, G.R., Kim, S.K., 2012. Neonatal beta cell development in mice and humans is regulated by calcineurin/NFAT. Developmental Cell 23(1):21—34.

[22] Soleimanpour, S.A., Crutchlow, M.F., Ferrari, A.M., Raum, J.C., Groff, D.N., Rankin, M.M., et al., 2010. Calcineurin signaling regulates human islet {beta}-cell survival. Journal of Biological Chemistry 285(51):40050—40059.

[23] Westacott, M.J., Ludin, N.W.F., Rkp, Benninger, 2017. Spatially organized beta-cell subpopulations control electrical dynamics across islets of langerhans. Biophysical Journal 113(5):1093—1108.

[24] Koster, J.C., Remedi, M.S., Flagg, T.P., Johnson, J.D., Markova, K.P., Marshall, B.A., et al., 2002. Hyperinsulinism induced by targeted suppression of beta cell KATP channels. Proceedings of the National Academy of Sciences of the U S A 99(26):16992—16997.

[25] Scharp, D.W., Kemp, C.B., Knight, M.J., Ballinger, W.F., Lacy, P.E., 1973. The use of ficoll in the preparation of viable islets of langerhans from the rat pancreas. Transplantation 16(6):686—689.

[26] Antonucci, S., Tagliavini, A., Pedersen, M.G., 2015. Reactive oxygen and nitrogen species disturb Ca(2+) oscillations in insulin-secreting MIN6 beta-cells. Islets 7(4):e1107255.

[27] Landa Jr., L.R., Harbeck, M., Kaihara, K., Chepurny, O., Kitiphongspattana, K., Graf, O., et al., 2005. Interplay of Ca2+ and cAMP signaling in the insulin-secreting MIN6 beta-cell line. Journal of Biological Chemistry 280(35): 31294—31302.

[28] Liu, Y.J., Tengholm, A., Grapengiesser, E., Hellman, B., Gylfe, E., 1998. Origin of slow and fast oscillations of Ca2+ in mouse pancreatic islets. Journal of Physiology 508(Pt 2):471—481.

[29] Heinz, S., Benner, C., Spann, N., Bertolino, E., Lin, Y.C., Laslo, P., et al., 2010. Simple combinations of lineage-determining transcription factors prime cis-regulatory elements required for macrophage and B cell identities. Molecular Cell 38(4):576—589.

[30] Bailey, T.L., Johnson, J., Grant, C.E., Noble, W.S., 2015. The MEME suite. Nucleic Acids Research 43(W1):W39—W49.

[31] Grant, C.E., Bailey, T.L., Noble, W.S., 2011. FIMO: scanning for occurrences of a given motif. Bioinformatics 27(7):1017—1018.

[32] Neph, S., Kuehn, M.S., Reynolds, A.P., Haugen, E., Thurman, R.E., Johnson, A.K., et al., 2012. BEDOPS: high-performance genomic feature operations. Bioinformatics 28(14):1919—1920.

[33] Quinlan, A.R., Hall, I.M., 2010. BEDTools: a flexible suite of utilities for comparing genomic features. Bioinformatics 26(6):841—842.

[34] Ishihara, H., Asano, T., Tsukuda, K., Katagiri, H., Inukai, K., Anai, M., et al., 1993. Pancreatic beta cell line MIN6 exhibits characteristics of glucose metabolism and glucose-stimulated insulin secretion similar to those of normal islets. Diabetologia 36(11):1139—1145.

[35] Palmer, A.E., Giacomello, M., Kortemme, T., Hires, S.A., Lev-Ram, V., Baker, D., et al., 2006. Ca2+ indicators based on computationally redesigned calmodulin-peptide pairs. Chemical Biology 13(5):521—530.

[36] Crabtree, G.R., Olson, E.N., 2002. NFAT signaling: choreographing the social lives of cells. Cell 109(Suppl):S67—S79.

[37] Macian, F., 2005. NFAT proteins: key regulators of T-cell development and function. Nature Reviews Immunology 5(6):472—484.

[38] Lawrence, M.C., McGlynn, K., Shao, C., Duan, L., Naziruddin, B., Levy, M.F., et al., 2008. Chromatin-bound mitogen-activated protein kinases transmit dynamic signals in transcription complexes in beta-cells. Proceedings of the National Academy of Sciences of the U S A 105(36):13315—13320.

[39] Koch, G.L., 1990. The endoplasmic reticulum and calcium storage. BioEssays 12(11):527—531.

[40] Lam, A.K., Galione, A., 2013. The endoplasmic reticulum and junctional membrane communication during calcium signaling. Biochimica et Biophysica Acta 1833(11):2542—2559.

[41] Varadi, A., Rutter, G.A., 2002. Dynamic imaging of endoplasmic reticulum Ca2+ concentration in insulin-secreting MIN6 Cells using recombinant targeted cameleons: roles of sarco(endo)plasmic reticulum Ca2+-ATPase (SERCA)-2 and ryanodine receptors. Diabetes 51(Suppl 1):S190—S201.

[42] Wang, R., McGrath, B.C., Kopp, R.F., Roe, M.W., Tang, X., Chen, G., et al., 2013. Insulin secretion and Ca2+ dynamics in beta-cells are regulated by PERK (EIF2AK3) in concert with calcineurin. Journal of Biological Chemistry 288(47):33824—33836.

[43] Caldwell, J.H., Herin, G.A., Nagel, G., Bamberg, E., Scheschonka, A., Betz, H., 2008. Increases in intracellular calcium triggered by channelrhodopsin-2 potentiate the response of metabotropic glutamate receptor mGluR7. Journal of Biological Chemistry 283(36):24300—24307.

[44] Briant, L.J.B., Reinbothe, T.M., Spiliotis, I., Miranda, C., Rodriguez, B., Rorsman, P., 2018. delta-cells and beta-cells are electrically coupled and regulate alpha-cell activity via somatostatin. Journal of Physiology 596(2): 197—215.

[45] Reinbothe, T.M., Safi, F., Axelsson, A.S., Mollet, I.G., Rosengren, A.H., 2014. Optogenetic control of insulin secretion in intact pancreatic islets with beta-cell-specific expression of Channelrhodopsin-2. Islets 6(1):e28095.

[46] Hannanta-Anan, P., Chow, B.Y., 2016. Optogenetic control of calcium oscillation waveform defines NFAT as an integrator of calcium load. Cells and System 2(4):283—288.

[47] Westacott, M.J., Ludin, N., Benninger, R.K.P., 2017. Spatially organized subpopulations of cells control electrical activity and dynamics across the islets of Langerhans. Biophyscial Journal.

[48] Miranda, J.G., Weaver, A.L., Qin, Y., Park, J.G., Stoddard, C.I., Lin, M.Z., et al., 2012. New alternately colored FRET sensors for simultaneous monitoring of Zn(2)(+) in multiple cellular locations. PLoS One 7(11):e49371.

[49] Kotla, S., Singh, N.K., Kirchhofer, D., Rao, G.N., 2017. Heterodimers of the transcriptional factors NFATc3 and FosB mediate tissue factor expression for 15(S)-hydroxyeicosatetraenoic acid-induced monocyte trafficking. Journal of Biological Chemistry 292(36):14885—14901.

[50] Ray, J.D., Kener, K.B., Bitner, B.F., Wright, B.J., Ballard, M.S., Barrett, E.J., et al., 2016. Nkx6.1-mediated insulin secretion and beta-cell proliferation is dependent on upregulation of c-Fos. FEBS Letters 590(12):1791–1803.

[51] Wild, A.R., Sinnen, B.L., Dittmer, P.J., Kennedy, M.J., Sather, W.A., Dell'Acqua, M.L., 2019. Synapse-to-Nucleus communication through NFAT is mediated by L-type Ca(2+) channel Ca(2+) spike propagation to the soma. Cell Reports 26(13):3537–35350 e4.

[52] Farnsworth, N.L., Benninger, R.K., 2014. New insights into the role of connexins in pancreatic islet function and diabetes. FEBS Letters 588(8):1278–1287.

[53] Arda, H.E., Li, L., Tsai, J., Torre, E.A., Rosli, Y., Peiris, H., et al., 2016. Age-dependent pancreatic gene regulation reveals mechanisms governing human beta cell function. Cell Metabolism 23(5):909–920.

[54] Berthault, C., Staels, W., Scharfmann, R., 2020. Purification of pancreatic endocrine subsets reveals increased iron metabolism in beta cells. Molecular Metabolism 42:101060.

[55] DiGruccio, M.R., Mawla, A.M., Donaldson, C.J., Noguchi, G.M., Vaughan, J., Cowing-Zitron, C., et al., 2016. Comprehensive alpha, beta and delta cell transcriptomes reveal that ghrelin selectively activates delta cells and promotes somatostatin release from pancreatic islets. Molecular Metabolism 5(7):449–458.

[56] Dorrell, C., Schug, J., Canaday, P.S., Russ, H.A., Tarlow, B.D., Grompe, M.T., et al., 2016. Human islets contain four distinct subtypes of beta cells. Nature Communications 7:11756.

[57] Farnsworth, N.L., Hemmati, A., Pozzoli, M., Benninger, R.K., 2014. Fluorescence recovery after photobleaching reveals regulation and distribution of connexin36 gap junction coupling within mouse islets of Langerhans. Journal of Physiology 592(20):4431–4446.

[58] Kono, T., Tong, X., Taleb, S., Bone, R.N., Iida, H., Lee, C.C., et al., 2018. Impaired store-operated calcium entry and STIM1 loss lead to reduced insulin secretion and increased endoplasmic reticulum stress in the diabetic beta-cell. Diabetes 67(11):2293–2304.

[59] Camunas-Soler, J., Dai, X.Q., Hang, Y., Bautista, A., Lyon, J., Suzuki, K., et al., 2020. Patch-seq links single-cell transcriptomes to human islet dysfunction in diabetes. Cell Metabolism 31(5):1017–10131 e4.

[60] Hodson, D.J., Mitchell, R.K., Bellomo, E.A., Sun, G., Vinet, L., Meda, P., et al., 2013. Lipotoxicity disrupts incretin-regulated human beta cell connectivity. Journal of Clinical Investigation 123(10):4182–4194.

[61] Dula, S.B., Jecmenica, M., Wu, R., Jahanshahi, P., Verrilli, G.M., Carter, J.D., et al., 2010. Evidence that low-grade systemic inflammation can induce islet dysfunction as measured by impaired calcium handling. Cell Calcium 48(2–3):133–142.

[62] Ramadan, J.W., Steiner, S.R., O'Neill, C.M., Nunemaker, C.S., 2011. The central role of calcium in the effects of cytokines on beta-cell function: implications for type 1 and type 2 diabetes. Cell Calcium 50(6):481–490.

[63] Clair JR, St., Westacott, M.J., Farnsworth, N.L., Kravets, V., Schleicher, W.E., Miranda, J.G., et al., 2020. Restoring connexin-36 function in diabetogenic environments precludes mouse and human islet dysfunction. bioRxiv.

[64] Wang, P., Alvarez-Perez, J.C., Felsenfeld, D.P., Liu, H., Sivendran, S., Bender, A., et al., 2015. A high-throughput chemical screen reveals that harmine-mediated inhibition of DYRK1A increases human pancreatic beta cell replication. Nature Medicine 21(4):383–388.

[65] Dolmetsch, R.E., Xu, K., Lewis, R.S., 1998. Calcium oscillations increase the efficiency and specificity of gene expression. Nature 392(6679):933–936.

[66] Liang, K., Du, W., Lu, J., Li, F., Yang, L., Xue, Y., et al., 2014. Alterations of the Ca(2)(+) signaling pathway in pancreatic beta-cells isolated from db/db mice. Protein Cell 5(10):783–794.

[67] Bergsten, P., 1995. Slow and fast oscillations of cytoplasmic Ca2+ in pancreatic islets correspond to pulsatile insulin release. American Journal of Physiology 268(2 Pt 1):E282–E287.

[68] Keller, M.P., Paul, P.K., Rabaglia, M.E., Stapleton, D.S., Schueler, K.L., Broman, A.T., et al., 2016. The transcription factor Nfatc2 regulates beta-cell proliferation and genes associated with type 2 diabetes in mouse and human islets. PLoS Genetics 12(12):e1006466.

[69] Kolic, J., Beet, L., Overby, P., Cen, H.H., Panzhinskiy, E., Ure, D.R., et al., 2020. Differential effects of voclosporin and tacrolimus on insulin secretion from human islets. Endocrinology 161(11).

[70] Rajadhyaksha, A., Barczak, A., Macias, W., Leveque, J.C., Lewis, S.E., Konradi, C., 1999. L-Type Ca(2+) channels are essential for glutamate-mediated CREB phosphorylation and c-fos gene expression in striatal neurons. Journal of Neuroscience 19(15):6348–6359.

[71] Sheng, M., McFadden, G., Greenberg, M.E., 1990. Membrane depolarization and calcium induce c-fos transcription via phosphorylation of transcription factor CREB. Neuron 4(4):571–582.

[72] Sun, X., Lin, Y., 2016. Npas4: linking neuronal activity to memory. Trends in Neurosciences 39(4):264–275.

[73] Zhang, S.J., Zou, M., Lu, L., Lau, D., Ditzel, D.A., Delucinge-Vivier, C., et al., 2009. Nuclear calcium signaling controls expression of a large gene pool: identification of a gene program for acquired neuroprotection induced by synaptic activity. PLoS Genetics 5(8):e1000604.

[74] Simonett, S.P., Shin, S., Herring, J.A., Bacher, R., Smith, L.A., Dong, C., et al., 2021. Identification of direct transcriptional targets of NFATC2 that promote beta-cell proliferation. Journal of Clinical Investigation.

[75] Remedi, M.S., Kurata, H.T., Scott, A., Wunderlich, F.T., Rother, E., Kleinridders, A., et al., 2009. Secondary consequences of beta cell inexcitability: identification and prevention in a murine model of K(ATP)-induced neonatal diabetes mellitus. Cell Metabolism 9(2):140–151.

[76] Stancill, J.S., Cartailler, J.P., Clayton, H.W., O'Connor, J.T., Dickerson, M.T., Dadi, P.K., et al., 2017. Chronic beta-cell depolarization impairs beta-cell identity by disrupting a network of Ca(2+)-regulated genes. Diabetes 66(8): 2175–2187.

[77] Benninger, R.K., Hutchens, T., Head, W.S., McCaughey, M.J., Zhang, M., Le Marchand, S.J., et al., 2014. Intrinsic islet heterogeneity and gap junction coupling determine spatiotemporal Ca(2)(+) wave dynamics. Biophysical Journal 107(11):2723–2733.

[78] Speckmann, T., 2019. The role of Npas4 and Rgs2 in the regulation of pancreatic β-cell function. University of British Columbia. https://doi.org/10.14288/1.0380061.

[79] Head, W.S., Orseth, M.L., Nunemaker, C.S., Satin, L.S., Piston, D.W., Benninger, R.K., 2012. Connexin-36 gap junctions regulate in vivo first- and second-phase insulin secretion dynamics and glucose tolerance in the conscious mouse. Diabetes 61(7):1700–1707.

[80] Ravier, M.A., Guldenagel, M., Charollais, A., Gjinovci, A., Caille, D., Sohl, G., et al., 2005. Loss of connexin36 channels alters beta-cell coupling, islet synchronization of glucose-induced Ca2+ and insulin oscillations, and basal insulin release. Diabetes 54(6):1798–1807.

[81] Benninger, R., Hodson, D.J., 2018. New understanding of beta-cell heterogeneity and in situ islet function. Diabetes 67(4):537–547.

[82] Bader, E., Migliorini, A., Gegg, M., Moruzzi, N., Gerdes, J., Roscioni, S.S., et al., 2016. Identification of proliferative and mature beta-cells in the islets of Langerhans. Nature 535(7612):430–434.

